Author Manuscript

Author Manuscript

Author Manuscript

Author Manuscript

HHS Public Access

Author manuscript

Cryst Growth Des. Author manuscript; available in PMC 2018 June 27.

Published in final edited form as:

Cryst Growth Des. 2018 January 3; 18(1): 85–94. doi:10.1021/acs.cgd.7b00878.

Optimizing Crystal Size of Photosystem II by Macroseeding: Toward Neutron Protein Crystallography

Rana Hussein[*,†], **Mohamed Ibrahim**[†], **Ruchira Chatterjee**[‡], **Leighton Coates**[#], **Frank Müh**[§], **Vittal K. Yachandra**[‡], **Junko Yano**[‡], **Jan Kern**[‡], **Holger Dobbek**[†], and **Athina Zouni**[*,†]

[†]Institut für Biologie, Humboldt-Universität zu Berlin, Unter den Linden 6, D-10099 Berlin, Germany

[‡]Molecular Biophysics and Integrated Bioimaging Division, Lawrence Berkeley National Laboratory, Berkeley, California 94720, United States

[#]Neutron Scattering Science Division, Oak Ridge National Laboratory, 1 Bethel Valley Road, Oak Ridge, Tennessee 37831, United States

[§]Institute of Theoretical Physics, Johannes Kepler University Linz, Linz, Austria

Abstract

Photosystem II (PSII) catalyzes the photo-oxidation of water to molecular oxygen and protons. The water splitting reaction occurs inside the oxygen-evolving complex (OEC) via a Mn_4CaO_5 cluster. To elucidate the reaction mechanism, detailed structural information for each intermediate state of the OEC is required. Despite the current high-resolution crystal structure of PSII at 1.85 Å and other efforts to follow the structural changes of the Mn_4CaO_5 cluster using X-ray free electron laser (XFEL) crystallography in addition to spectroscopic methods, many details about the reaction mechanism and conformational changes in the catalytic site during water oxidation still remain elusive. In this study, we present a rarely found successful application of the conventional macroseeding method to a large membrane protein like the dimeric PSII core complex (dPSIIcc). Combining microseeding with macroseeding crystallization techniques allowed us to reproducibly grow large dPSIIcc crystals with a size of ~3 mm. These large crystals will help improve the data collected from spectroscopic methods like polarized extended X-ray absorption fine structure (EXAFS) and single crystal electron paramagnetic resonance (EPR) techniques and are a prerequisite for determining a three-dimensional structure using neutron diffraction.

[*]Corresponding Authors: (R.H.) Phone; +49 30 2093 47933; husseinr@huberlin.de. (A.Z.) Phone: +49 30 2093 47930; athina.zouni@huberlin.de.

ORCID

Rana Hussein: 0000-0001-6292-2375
Mohamed Ibrahim: 0000-0002-1431-9755
Frank Müh: 0000-0002-8818-2616
Junko Yano: 0000-0001-6308-9071
Holger Dobbek: 0000-0002-4122-3898
Athina Zouni: 0000-0003-0561-6990

Notes

The authors declare no competing financial interest.

The Supporting Information is available free of charge on the ACS Publications website at DOI: 10.1021/acs.cgd.7b00878. Figure S1 shows DEAE anion exchange column chromatography for purifying βDM dPSIIcc, gel filtration chromatography of dPSIIcc in Figure S2, microcrystals produced from precrystallization in Figure S3, DLS measurement of purified dPSIIcc in Figure S4, measuring PEG 2000 concentration using reffective index in Figure S5 and Table S1 (PDF)

Author Manuscript Author Manuscript Author Manuscript Author Manuscript

Graphical Abstract

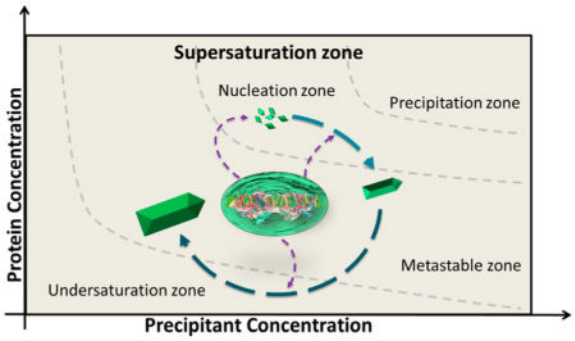

1. INTRODUCTION

Oxygenic photosynthesis is considered the basis for aerobic life on earth. It provides us with food and the oxygen present in our atmosphere. The light reactions of oxygenic photosynthesis take place mainly in two major protein complexes: photosystem II (PSII) and photosystem I (PSI). PSII and PSI have a unique capability to utilize light energy through performing light-induced charge separation and convert it into molecular oxygen and the stored chemical energy used to build up carbohydrates.[1,2]

PSII is a large multisubunit protein complex located in the thylakoid membranes of cyanobacteria, green algae, and higher plants. It acts as water–plastoquinone–oxidoreductase, catalyzing the electron extraction from water molecules[3,4] coupled with the reduction of its final electron acceptor, a plastoquinone.[5] In cyanobacteria, the photosystem II core complex (PSIIcc) is typically homodimeric.[6–8] Each monomer has a molecular mass of 350 kDa and consists of a total of 20 subunits, of which 17 are membrane-intrinsic and 3 are membrane-extrinsic located at the lumenal side.[2,9,10] The PSII reaction center core consists of a heterodimer of the transmembrane subunits D1 (PsbA) and D2 (PsbD), harboring all of the redox-active cofactors necessary for the electron transfer and water splitting reactions, and is flanked by the two other large subunits CP47 (PsbB) and CP43 (PsbC). Central to water splitting in PSII is the oxygen-evolving complex (OEC) located at the lumenal side and ligated by carboxylate and histidine ligands of the D1 and CP43 subunits. The OEC consists of a cluster having four manganese (Mn) ions and one calcium (Ca) ion connected by μ-oxo bridges (Mn_4CaO_5 cluster).[2,11] This metal complex cycles through five different intermediate states, known as S states (S0, S1, S2, S3, and S4), to facilitate the extraction of four electrons and four protons from two water molecules to form one dioxygen molecule.[12–14]

Elucidating how the electronic and geometric structures change in the OEC during catalysis at each S state will pave the way for a better understanding of the mechanism of water splitting and the formation of the O–O bond. The occurrence of structural changes during water oxidation has been demonstrated by several biochemical and biophysical techniques, including X-ray crystallography,[10,11,15–25] Fourier transform IR spectroscopy (FTIR),[26–29] extended X-ray absorption fine structure (EXAFS),[4,30–37] and electron paramagnetic

Author Manuscript Author Manuscript Author Manuscript Author Manuscript

resonance (EPR).[38–45] The atomic resolution crystal structure of dPSIIcc in the dark stable S1 state from *Thermosynechococcus (T.) vulcanus* at 1.9 Å showed that the core of the metal cluster has the overall shape of a distorted chair.[9,11] This distorted chair is formed by three Mn ions (Mn1–Mn3), four oxygen atoms (O1–O3 and O5), and one calcium ion, whereas the fourth Mn ion is located outside and is connected via μ-oxo-bridges through O4 and O5. Additionally, two water molecules are assigned to coordinate Mn4 (W1 and W2) and another two water molecules coordinate the calcium ion (W3, W4).[11] The geometry of the Mn_4CaO_5 cluster revealed by the X-ray crystal structures[11,22,25] is an important step on the way to fathom the water splitting mechanism. EXAFS data collected from protein solutions, oriented membranes and single crystals provided precise information about metal-to-metal distances (Mn–Mn and Mn–Ca) and metal-to-ligand distances (Mn–O) with less reduction by X-ray radiation than the X-ray diffraction data.[4] In addition, EPR data gave insights into the electronic structure for the different intermediates of the metal cluster.[43,46–48] But despite all the improvements in understanding the structure of the OEC using several approaches, the dynamic mechanism of water oxidization by PSII still remains elusive. In addition to the accurate location of the Mn ions, Ca^{2+}, bridging oxygen, and the water molecules, we also need to resolve the protonation pattern surrounding the OEC.

In this study, macroseeding in a combination with microseeding is introduced under “PEG-out conditions” to produce large single crystals of dPSIIcc. These large crystals are ideal samples to improve the quality of the data obtained from various orientation-dependent spectroscopic techniques that require highly concentrated protein sample like polarized EXAFS[49] and single crystal EPR.[50,51] Using these crystals will help to enhance the signal-to-noise ratio (S/N) and to provide accurate measurements for each orientation. Therefore, having these large crystals will be very useful to extend the spectroscopic investigation of PSII. Furthermore, these dPSIIcc macrocrystals will help to overcome one of the main obstacles in applying neutron diffraction crystallography. Neutron diffraction studies are complementary to X-ray diffraction analysis. However, they require very large crystals (>1 mm^3) in order to compensate for the weak beam flux of the available neutron sources.[52,53] Through applying neutron diffraction on PSII, radiation damage that usually happens through using synchrotron X-ray sources[54] will be completely avoided. In addition, neutron diffraction has the ability to visualize protons and can, therefore, help in mapping out water transport channels and revealing details of the hydrogen-bonding network surrounding the OEC, which is difficult to reveal using X-ray diffraction.[52,55–58] We note that the quality of trimeric photosystem I (tPSI) crystals was improved by using a protocol based on the combination of micro- and macroseeding techniques under “reverse salting-in” conditions that was developed in 1998 by Fromme and Witt.[59] The improved tPSI crystals obtained by this protocol have been applied in both X-ray structure analysis[60] and electron spin resonance spectroscopy.[61]

We developed a fast and reproducible macroseeding protocol, which results in the formation of dPSIIcc crystals of ~1.8 mm length in the long axis within ~2–3 days. Utilizing repeated seeding, we also produced larger dPSIIcc crystals of ~3 mm along the long axis. The details of the developed protocol are discussed in detail in this study. Starting point for this protocol is medium size crystals within the size range of 100 μm that are used as seeds after being washed in a pre-equilibrated drop containing dPSIIcc solution. The growth of too many

Author Manuscript Author Manuscript Author Manuscript Author Manuscript

crystals in the initial step of the crystal growth, which is known to be a general problem of macroseeding techniques,[62,63] was overcome by widening the metastable zone. Hanging drop plates were used to avoid crystals adhering to the wall of the plates and further possible mechanical damage that may happen when trying to transfer these large crystals. The generated dPSIIcc macrocrystals were examined by means of X-ray diffraction measurements at the Synchrotron (BESSY II, Berlin). Furthermore, the first neutron diffraction measurements on hydrogen/deuterium exchanged dPSIIcc macrocrystals were performed at the MaNDi instrument at the Spallation Neutron Source at Oak Ridge National Laboratory (ORNL, USA).

2. EXPERIMENTAL PROCEDURES

2.1. Cell Growth and Protein Purification

Cells of *Thermosynechococcus elongatus* BP-1 were grown and thylakoid membranes were prepared according to Kern et al.[7] Dimeric PSIIcc (dPSIIcc) and trimeric PSI (tPSI) were extracted from the thylakoid membranes using *n*-dodecyl-*β*-D-maltoside (*β*DM) as a detergent but with a concentration of 2% instead of 0.55%. PSIIcc and the trimeric PSI were separated chromatographically using a weak anion exchanger column (ToyoPearl DEAE; see Figure S1A). The higher concentration of 2% *β*DM for the extraction results in a dramatic increase of the amount of extracted tPSI: It increased by a factor of 3 compared to using 0.55% *β*DM (Figure S1). Interestingly, this is accompanied by a significant increase of the amount of the dPSIIcc compared to the monomeric form (mPSIIcc; Figure S2), usually a 1:1 ratio of PSIIcc monomer to dimer after purifying by DEAE column chromatography was obtained using 0.55% *β*DM during extraction. In comparison, using 2% *β*DM during extraction gave almost pure dPSIIcc and the monomeric form was rarely detected. These results are consistent with the results reported by Watanabe et al.[64] showing that the amount of dPSIIcc extracted relative to mPSIIcc increases with increasing the concentration of *β*DM from 0.5% to 2%. After the chromatography step, the fraction containing dPSIIcc was concentrated using Vivaspin ultrafiltration spin columns (Sartorious, Germany) with a cutoff of 100 kDa. The protein samples were washed twice with 100 mM PIPES (1,4-piperazinediethanesulfonic acid), pH 7.0, 5 mM $CaCl_2$, 5% glycerol, and 0.02% *β*DM. Monodispersity and the homogeneity of dPSIIcc were enhanced by precrystallization at 0.75 mM chlorophyll (Chl) *a* concentration (equivalent to 8 mg/mL protein) for 12 h at 4 °C.[7] The microcrystals of dPSIIcc (Figure S3) were collected and resolubilized followed by washing and concentrating to 4 mM Chl *a* (equivalent to 42.8 mg/mL protein). Then the sample was directly frozen and stored in liquid nitrogen. This precrystallization step was repeated twice and monitored by dynamic light scattering (DLS Wyatt Dynapro with 787 nm laser wavelength). These two precrystallization steps decrease the polydispersity of dPSIIcc from ~24% to ~12% (see Figure S4).

2.2. dPSIIcc Protein Concentrations Via Chl a Concentrations

Chl *a* concentration of dPSIIcc samples were determined as usual by extraction in 80% aqueous acetone and using the extinction coefficient $\varepsilon_{(663nm)} = 74.000\ M^{-1}\ cm^{-1}$. As each dPSIIcc contains 70 Chl *a* pigment molecules, the dPSIIcc concentration is given by

Author Manuscript Author Manuscript Author Manuscript Author Manuscript

$$\text{dPSIIcc conc. in g/L} = \frac{\text{Chl } a \text{ conc. in mol/L}}{70} \times 750.000$$

where 750.000 g/mol is the molecular mass of dPSIIcc.

2.3. Oxygen-Evolving Activity

Oxygen evolution activity of the purified dPSIIcc was assessed at room temperature (RT) using a Clark-type electrode (OxyLab, Hansatech instruments). All the measurements were performed under saturating light conditions to guarantee the independence of light intensity. The dPSIIcc samples were diluted to a final concentration of 2–5 μM Chl *a* (equivalent to 21.4–53.5 mg mL^{-1} protein concentration) using MCM buffer (20 mM MES/NaOH, pH 6.5, 20 mM $CaCl_2$, 10 mM $MgCl_2$). The artificial electron acceptor DCPQ (2,5-dichloro-*p*-benzoquinone) was added to the protein mixture at a final concentration of 3 μM. The Clark electrode was calibrated against air-saturated water and nitrogen-saturated water at atmospheric pressure at RT. The final dPSIIcc samples used for crystallization showed oxygen evolution activity rates ranging from 2900 to 4500 μmol O_2 (mg Chl *a* h)$^{-1}$.

2.4. Protein Crystallization and Studying the Phase Diagram

The phase diagram of the dPSIIcc/PEG 2000 system (Figure 1) was determined using a range of protein concentrations from 1 mM to 5 mM Chl *a* (equivalent to 10.7–53.5 mg/mL protein). The dPSIIcc protein dissolved in a buffer containing 100 mM PIPES, pH 7.0, 5 mM $CaCl_2$, 5% glycerol, and 0.03% βDM was crystallized by mixing 1:1 with the crystallization buffer containing 100 mM PIPES, pH 7.0, 5 mM $CaCl_2$, 5% glycerol and 5–10% (w/v) of polyethylene glycol (PEG) 2000 as precipitant. Sitting drop crystallization plates (Hampton Research, USA) were used, and 1 mL of the crystallization buffer was added to the reservoir. All crystallization steps were done at 20 °C. Wells that did not show any crystal growth after 24 h incubation time were seeded with a single microcrystal (~50 μm) to differentiate between the unsaturated and the metastable zones.

2.5. Increasing the Width of the Metastable Zone

The unsaturated, the metastable, and the labile zones of the dPSIIcc were identified at a Chl *a* concentration of 2 mM (final concentration after mixing with the crystallization buffer). The crystallization buffers contained different concentrations of $CaCl_2$ (5 mM, 10 mM, 20 mM, 40 mM) and PEG 2000 (5–7.6%; see Figure 2). Sitting drop crystallization plates (Hampton Research, USA) were used. Two microliters of the protein solution at 4 mM Chl *a* (equivalent to 42.8 mg/mL protein) was mixed with the crystallization buffer in a ratio of 1:1, and 1 mL of the crystallization buffer was added to the reservoir.

2.6. Controlling the Concentration of PEG 2000 in the Crystallization Buffer

Precise PEG 2000 concentrations in the crystallization buffer were determined by measuring the refractive index (RI) using an Abbe refractometer (KRÜSS, model: AR2008). The standard curve was recorded at RT (20 °C) for a wide range of different PEG 2000 concentrations (0–10%) in the crystallization buffer (see Figure S5 and Table S1). Five microliters from each buffer prepared were used to measure the RI, and the corresponding

Author Manuscript Author Manuscript Author Manuscript Author Manuscript

concentration of PEG 2000 was calculated from the standard curve. The error in the concentration was approximately ±0.15%.

2.7. Macrocrystals Preparation

2.7.1. Microseeds Preparation—The dPSIIcc microseeding stock was prepared as described by Ibrahim et al.[65] A group of dPSIIcc crystals (around 5–7 crystals in the size range of 400 μm) was transferred to an Eppendorf tube and filled up to 500 μL with the crystallization buffer containing 6% PEG 2000 and 0.03% βDM. A seed toolkit (Hampton Research, USA) was used to crush the crystals by vortexing for a few minutes. The protein was mixed with the seed stock at a ratio of 1:4. Crystals were grown using hanging or sitting drop plates (Hampton Research, USA). One milliliter of the crystallization buffer containing 6% PEG 2000 was added to the reservoir (Figure 3). Medium-sized dPSIIcc crystals were produced at 20 °C within 4–5 h (Figure 4).

2.7.2. Steps of Macroseeding—Day one (protein equilibration): The dPSIIcc protein at a concentration of 2 mM Chl *a* (equivalent to 21.4 mg/mL protein) was equilibrated in the metastable zone with crystallization buffer containing 20 mM $CaCl_2$ and 6.5–6.8% PEG 2000. Drops were equilibrated by vapor diffusion for 1 day at 20 °C in sitting drop plates (Hampton Research, USA).

Day two: Each crystal prepared by microseeding (see section 2.7.1) with a size of 100–150 μm was washed in several steps going from high to low concentration of PEG 2000 (from 8% to 4%) in the crystallization buffer. This washing step aimed at removing the extraneous nuclei from crystals. The washed crystal was then transferred to 4 μL of the equilibrated dPSIIcc drop with a total concentration of 8 mM Chl *a* (equivalent to 85.6 mg/mL protein) per drop. The equilibrated drop containing the washed crystal was then transferred quickly to the silicone-greased coverslip (Marienfeld, Germany) and sealed above the hanging drop well (Hampton, USA) containing 1 mL of the crystallization buffer with the same concentration of PEG 2000 that had been used during protein equilibration (Figure 5). The dPSIIcc seed crystals in the equilibrated dPSIIcc solution were grown slowly within 2–3 days at 20 °C.

2.8. Crystallographic Data Collection

The large crystals obtained were partially dehydrated by placing 1 mL of a buffer containing 100 mM PIPES, pH 7.0, 20 mM $CaCl_2$, 25% PEG 2000, 30% glycerol in the reservoir of the hanging drop plate for 1 day. Finally, the crystals were incubated in that buffer for 30 min and afterward directly flash-cooled in a nitrogen gas stream at 100 K. X-ray diffraction (XRD) measurements were performed under cryogenic conditions at beamline 14.1 operated by the Helmholtz-Zentrum Berlin (HZB) at the BESSY II electron storage ring (Berlin, Germany).[66] The data set was collected at 0.91841 Å X-ray wavelength and integrated and scaled with XDS[67] and XDSAPP.[66]

Author Manuscript Author Manuscript Author Manuscript Author Manuscript

2.9. Procedure of Hydrogen/Deuterium Exchange in dPSIIcc Macrocrystals and Neutron Diffraction Measurement

The dPSIIcc macrocrystals were grown in hanging drop plates (Hampton Research, USA) until they reached a size of approximately 2 mm as described in section 2.7.2. The buffer in the reservoir was exchanged with a buffer completely prepared using D_2O (100 mM PIPES, pD 7.0, 20 mM $CaCl_2$, 10% PEG 2000). After 2 days, the crystals were partially dehydrated by gradually increasing the PEG 2000 concentration in the deuterated buffer until reaching 30%. All crystals were left for another 2 days followed by being mounted and sealed in fused-silica capillaries with an inner diameter of 2 mm (Vitrocom, USA) along with a drop of the deuterated buffer. The crystals were then transported to the Spallation Neutron Source (SNS) at Oak Ridge National Laboratory (ORNL in Tennessee, USA) to test them at the Macromolecular Neutron Diffractometer (MaNDI) instrument.[68,69] The Laue neutron beam used in the experiment consisted of neutrons between 2.5 and 4.5 Å. Diffraction was detected using 40 SNS Anger cameras with a crystal to detector distance of 450 mm. MaNDi uses time-of-flight techniques[52] to separate Bragg reflections from a Laue experiment into wavelength-resolved monochromatic data slices. This technique reduces spatial overlap of reflections, which is vital for separating Bragg reflections from unit cells sizes above 150 Å[69] while also decreasing background and thus improving the signal-to-noise ratio for each reflection. A single ω angle was chosen for data collection and the crystal remained static during the 24 h exposure time at room temperature (295 K).

3. RESULTS AND DISCUSSION

3.1. Phase Diagram and Macrocrystallization of dPSIIcc

Understanding and identifying the phase diagram of dPSIIcc provides us with the necessary data for controlling the growth of dPSIIcc crystals. A phase diagram of dPSIIcc protein using the crystallization buffer containing 100 mM PIPES, pH 7.0, 5% glycerol, 5 mM $CaCl_2$ against PEG 2000 as a precipitant (see Figure 1) was determined using vapor diffusion as a crystallization technique, which was also used for macroseeding. The metastable zone (the saturation region), where the crystal growth is supported and no spontaneous nucleation is observed, was identified at different dPSIIcc concentrations between 0.5 and 2.5 mM Chl *a*. The width of this zone was within 1.46% of PEG 2000 on average for those particular protein concentrations (0.5 to 2.5 mM Chl *a*). The width of this zone is increasing with decreasing protein concentration reaching its maximum at a protein concentration of 0.5 mM Chl *a*. However, transferring a single crystal with size ~100 μm into an equilibrated dPSIIcc solution in the metastable zone at low protein concentration (0.5 mM Chl *a*) did not result in any visible growth of the crystal. After many trials of inserting a crystal to equilibrated drops with different protein concentrations (0.5 mM Chl *a* to 2 mM Chl *a*), dPSIIcc with 2 mM Chl *a* proved to be the most stable and reproducible concentration for crystal growth. The borders between the metastable zone and either the undersaturation region or the labile zone, where nucleation takes place, were identified to be below 5.3% of PEG 2000 and higher than 6.6%, respectively, for a protein concentration of 2 mM Chl *a*.

Author Manuscript Author Manuscript Author Manuscript Author Manuscript

3.2. Effect of $CaCl_2$ in Increasing the Metastable Zone Width for Macroseeding

The phase diagram determined in this study revealed the presence of a narrow metastable zone at different protein concentrations (see Figure 1). The metastable zone width varied between 1.2% and 1.8% of PEG 2000 for the dPSIIcc protein with 2.5 mM and 0.5 mM Chl *a*, respectively. Applying macroseeding steps at a dPSII concentration of 2 mM Chl *a* resulted in either dissolution of the inserted crystal in the equilibrated drop or in growth of too many small crystals in the drop and rarely yielded a single large macrocrystal. Previous work[70,71] has shown that salts like sodium chloride, potassium chloride, and calcium chloride can increase or decrease the width of the metastable zone. The effect can vary from buffer to buffer and from crystal type to crystal type. We studied the effect of $CaCl_2$ present in our crystallization buffer on the metastable zone by varying its concentration (5 mM, 10 mM, 20 mM, and 40 mM). As seen in Figure 2, the width of the metastable zone increases with increasing $CaCl_2$ concentrations. Consequently, increasing the $CaCl_2$ concentration also shifted the nucleation zone to a higher PEG 2000 concentration with little or no effect on the edge of the solubility border. The nucleation phase is shifted by 0.8% of PEG 2000 when using 40 mM instead of 5 mM $CaCl_2$, whereas the border between undersaturation and saturation zone is only shifted by 0.2% of PEG 2000.

3.3. Macrocrystallizations and Double Macrocrystallization of dPSIIcc

Crystal seeds for macroseeding act as a template on which further molecules of the protein will grow and assemble.[62] Homogeneity in the size and the quality of the crystal seed were achieved by applying the microseeding protocol developed by Ibrahim et al.[65] in which a group of well-shaped crystals suspended in the crystallization buffer having 6% PEG 2000 was smashed with the use of the seed bead (Figure 3) to prepare the seeding stock. The number of seeds in the crystallization buffer was optimized by several dilution steps for the seeding stock until reaching the optimal concentration. This procedure enables controlling the crystal size distribution resulting in growing medium-sized crystals with a uniformed size of ~100 μm within a few hours (Figure 4) from mixing the seeding stock with the protein. The solubility of these crystals was determined. It was found that the crystallization buffer containing 4% PEG 2000 represents the lowest concentration at which the crystals were stable for 15 to 20 min. On the basis of that, the extraneous layer of each single crystal was removed by transferring it into a series of four drops (500 μL each) containing the crystallization buffer with gradual decreasing the concentration of PEG 2000 from 8%, where the dPSIIcc crystal is completely stable, to 4%, where the crystal can melt completely. Each single crystal was incubated about 1 min in each drop and then transferred directly to 4 μL of an equilibrated dPSIIcc solution in the metastable zone. The crystal was left to grow for 2–3 days (Figure 5). On average, 60–70% of the seeded equilibrated drops yielded large macrocrystals with a size of ~1.8 mm along the long axis (Figure 6).

Crystallization buffers with different PEG 2000 concentrations have different refractive indices. Therefore, the refractive index (RI) was utilized to test each preparation of the crystallization buffer used for the protein equilibration in the metastable zone. In this way, the amount of dPSIIcc protein sample and time needed per setup was minimized. Also, we tried to maintain the shape of the drop on the coverslip to be as spherical as possible. As the equilibrated drop of dPSIIcc always contains 0.015% of βDM, it was challenging to keep the

Author Manuscript Author Manuscript Author Manuscript Author Manuscript

droplet shape uniform and well-structured, especially as all macroseeding steps needed to be carried out as quickly as possible. Different kinds of siliconized coverslips, as well as silicon oil, were tested. Unfortunately, none of these treatments gave stable, reproducible results. Finally, greasing the glass coverslip with silicone grease resulted in the formation of uniformly stable, spherical droplets (Figure 7).

In the double macroseeding protocol, the crystals resulting from the macroseeding with an average size of 1.5–2.0 mm were used as a seed in the next step. After being washed carefully, the crystals were transferred to a 10 μL equilibrated drop of dPSIIcc solution. The success rate in the double macroseeding was around 30%, and the crystals grew up to ~3.0 mm (Figure 8). The small success rate is due to difficult handling and transferring of the large crystals without inducing stress to them. Such stress and the handling often lead to contamination of the equilibrated drops with other tiny seeds resulting in growth of multiple crystals in the same drop.

3.4. Results of the X-ray Diffraction Studies

A rectangular-shaped single dPSIIcc crystal with the dimensions ≈2 mm × 0.60 mm × 0.40 mm was used for collecting a diffraction data set. The data set was processed to 4.11 Å resolution with a completeness of 88.9% (Table 1). The crystal belonged to the same space group as the unseeded βDM-dPSIIcc crystals,[10,15,17] having the orthorhombic space g roup $P2_12_12_1$ with unit cell constants a = 126.59 Å, b = 223.15 Å, c =305.46 Å. The diffraction pattern revealed clear diffraction spots without signs of twinning or the presence of polycrystals. It also showed an anisotropic diffuse background near the highest resolution shell (see Figure 9). The same is observed with the unseeded βDM dPSIIcc crystals.[7] This result indicates no significant difference between the unseeded and the seeded dPSIIcc crystals in terms of diffraction resolution.

Further improvements of the diffraction quality of the macrocrystals are currently planned by applying the macroseeding techniques developed in this work for the generation of dPSIIcc macrocrystals with the detergent $C_{12}E_8$ instead of βDM with subsequent postcrystallization treatment as described in the work of Hellmich et al.,[20] which reproducibly improves the resolution of our diffraction data sets.[20,23]

3.5. Results of Initial Neutron Diffraction Tests

A large single dPSIIcc crystal of ~2.0 mm × 0.8 mm × 0.3 mm generated using the macroseeding procedure was incubated in D_2O containing buffer (see section 2.9) to achieve partial D/H exchange and measured at the MaNDi instrument of the SNS at ORNL. Upon exposure for 24 h at room temperature, weak diffraction with a maximum resolution of ~8.0 Å was observed (Figure 10). These limited resolutions of 8–10 Å were due to nonoptimal deuteration of the crystals as well as limited crystal

volume given the large unit cell size of the dPSIIcc crystals. Further improvements in the neutron diffraction quality could be achieved by a more complete D/H exchange, including a complete exchange of the PEG and detergent against deuterated versions. These efforts are currently underway.

Author Manuscript Author Manuscript Author Manuscript Author Manuscript

4. CONCLUSION

Highly purified and monodisperse dPSIIcc solutions were prepared from the cyanobacterium *T. elongatus* BP-1 by solubilizing the thylakoid membrane with an approximately 4-fold higher concentration of detergent (βDM) compared to the standard procedure.[7] Using that monodisperse dPSIIcc sample with a combination of microseeding and macroseeding crystallization techniques, we were able to generate dPSIIcc macrocrystals. In this study, all the steps from both techniques were discussed in detail, demonstrating the ability to produce relatively fast growing macrocrystals. The width of the metastable zone was increased by increasing the concentration of calcium chloride, which provided us with a quite wide window for transferring the crystals into the pre-equilibrated drop of the protein and avoiding the growth of too many crystals in the beginning of the growth phase. The quality of the macro-sized crystals was tested using XRD. We collected an XRD data set from a βDM-dPSIIcc macrocrystal at 4.11 Å resolution. These large crystals will enhance the potential of collecting high-quality data from polarized spectroscopy techniques that require single crystals of PSII. They also represent another step toward obtaining a more detailed picture of the water environment surrounding the OEC using neutron diffraction.

Supplementary Material

Refer to Web version on PubMed Central for supplementary material.

Acknowledgments

Funding

This work was funded by the Human Frontiers Science Project Award No. RGP0063/2013 310 (R.H., A.Z, J.Y.), by Sonderforschungsbereich Sfb1078 (Humboldt Universität Berlin), Project A5 (MI, A.Z., H.D.), by Director, Office of Science, Office of Basic Energy Sciences (OBES), Division of Chemical Sciences, Geosciences, and Biosciences (CSGB) of the Department of Energy (DOE) under contract DE-AC02–05CH11231 (J.Y., V.K.Y.) and by National Institutes of Health (NIH) Grant GM055302 (V.K.Y.). A portion of this research used resources at the Spallation Neutron Source a DOE Office of Science User Facility operated by the Oak Ridge National Laboratory.

We acknowledge access to beamlines of the BESSY II storage ring (Berlin, Germany) via the Joint Berlin MX-Laboratory sponsored by the Helmholtz Zentrum Berlin für Materialien und Energie, the Freie Universität Berlin, the Humboldt-Universität zu Berlin, the Max-Delbrück-Centrum and the Leibniz-Institut für Molekulare Pharmakologie. We thank Dr. Martin Bommer for his support at BESSY and for helping in structure analyses, Ina Seuffert for technical assistance. We thank also the support staff at beamline 14.1 at the BESSY II and at MaNDi instrument at ORNL.

References

1. Nelson N, Yocum CF. Structure and function of photosystems I and II. Annu Rev Plant Biol. 2006; 57:521–565. [PubMed: 16669773]
2. Satoh, K., Wydrzynski, TJ. Photosystem II. Springer; 2005. Introduction to photosystem II; p. 11-22.
3. Muh F, Zouni A. Light-induced water oxidation in photosystem II. Front Biosci Landmark Ed. 2011; 16:3072–3132. [PubMed: 21622223]
4. Yano J, Yachandra V. Mn4Ca cluster in photosynthesis: where and how water is oxidized to dioxygen. Chem Rev. 2014; 114:4175–4205. [PubMed: 24684576]
5. Müh F, Glöckner C, Hellmich J, Zouni A. Light-induced quinone reduction in photosystem II. Biochim Biophys Acta, Bioenerg. 2012; 1817:44–65.

Author Manuscript Author Manuscript Author Manuscript Author Manuscript

6. Folea IM, Zhang P, Aro EM, Boekema EJ. Domain organization of photosystem II in membranes of the cyanobacterium *Synechocystis* PCC6803 investigated by electron microscopy. FEBS Lett. 2008; 582:1749–1754. [PubMed: 18466767]
7. Kern J, Loll B, Lüneberg C, DiFiore D, Biesiadka J, Irrgang KD, Zouni A. Purification, characterisation and crystallisation of photosystem II from *Thermosynechococcus elongatus* cultivated in a new type of photobioreactor. Biochim Biophys Acta, Bioenerg. 2005; 1706:147–157.
8. Shen JR, Kamiya N. Crystallization and the crystal properties of the oxygen-evolving photosystem II from *Synechococcus vulcanus*. Biochemistry. 2000; 39:14739–14744. [PubMed: 11101288]
9. Shen JR. The structure of photosystem II and the mechanism of water oxidation in photosynthesis. Annu Rev Plant Biol. 2015; 66:23–48. [PubMed: 25746448]
10. Guskov A, Kern J, Gabdulkhakov A, Broser M, Zouni A, Saenger W. Cyanobacterial photosystem II at 2.9-Å resolution and the role of quinones, lipids, channels and chloride. Nat Struct Mol Biol. 2009; 16:334–342. [PubMed: 19219048]
11. Umena Y, Kawakami K, Shen JR, Kamiya N. Crystal structure of oxygen-evolving photosystem II at a resolution of 1. 9 Å. Nature. 2011; 473:55–60. [PubMed: 21499260]
12. Kok B, Forbush B, McGloin M. Cooperation of charges in photosynthetic O2 evolution–I. A linear four step mechanism. Photochem Photobiol. 1970; 11:457–475. [PubMed: 5456273]
13. Joliot P. Period-four oscillations of the flash-induced oxygen formation in photosynthesis. Photosynth Res. 2003; 76:65–72. [PubMed: 16228566]
14. Dau H, Haumann M. The manganese complex of photosystem II in its reaction cycle—basic framework and possible realization at the atomic level. Coord Chem Rev. 2008; 252:273–295.
15. Zouni A, Witt HT, Kern J, Fromme P, Krauss N, Saenger W, Orth P. Crystal structure of photosystem II from *Synechococcus elongatus* at 3. 8 Å resolution. Nature. 2001; 409:739–743. [PubMed: 11217865]
16. Kamiya N, Shen JR. Crystal structure of oxygen-evolving photosystem II from *Thermosynechococcus vulcanus* at 3.7-Å resolution. Proc Natl Acad Sci U S A. 2003; 100:98–103. [PubMed: 12518057]
17. Loll B, Kern J, Saenger W, Zouni A, Biesiadka J. Towards complete cofactor arrangement in the 3. 0 Å resolution structure of photosystem II. Nature. 2005; 438:1040–1044. [PubMed: 16355230]
18. Kawakami K, Umena Y, Kamiya N, Shen JR. Location of chloride and its possible functions in oxygen-evolving photosystem II revealed by X-ray crystallography. Proc Natl Acad Sci U S A. 2009; 106:8567–8572. [PubMed: 19433803]
19. Kern J, Alonso-Mori R, Tran R, Hattne J, Gildea RJ, Echols N, Glöckner C, Hellmich J, Laksmono H, Sierra RG. Simultaneous femtosecond X-ray spectroscopy and diffraction of photosystem II at room temperature. Science. 2013; 340:491–495. [PubMed: 23413188]
20. Hellmich J, Bommer M, Burkhardt A, Ibrahim M, Kern J, Meents A, Müh F, Dobbek H, Zouni A. Native-like photosystem II superstructure at 2. 44 Å resolution through detergent extraction from the protein crystal. Structure. 2014; 22:1607–1615. [PubMed: 25438669]
21. Kern J, Tran R, Alonso-Mori R, Koroidov S, Echols N, Hattne J, Ibrahim M, Gul S, Laksmono H, Sierra RG. Taking snapshots of photosynthetic water oxidation using femtosecond X-ray diffraction and spectroscopy. Nat Commun. 2014; 5:4371. [PubMed: 25006873]
22. Suga M, Akita F, Hirata K, Ueno G, Murakami H, Nakajima Y, Shimizu T, Yamashita K, Yamamoto M, Ago H, Shen JR. Native structure of photosystem II at 1. 95 A resolution viewed by femtosecond X-ray pulses. Nature. 2015; 517:99–103. [PubMed: 25470056]
23. Young ID, Ibrahim M, Chatterjee R, Gul S, Fuller FD, Koroidov S, Brewster AS, Tran R, Alonso-Mori R, Kroll T. Structure of photosystem II and substrate binding at room temperature. Nature. 2016; 540:453–457. [PubMed: 27871088]
24. Suga M, Akita F, Sugahara M, Kubo M, Nakajima Y, Nakane T, Yamashita K, Umena Y, Nakabayashi M, Yamane T. Light-induced structural changes and the site of O= O bond formation in PSII caught by XFEL. Nature. 2017; 543:131–135. [PubMed: 28219079]
25. Tanaka A, Fukushima Y, Kamiya N. Two different structures of the oxygen-evolving complex in the same polypeptide frameworks of photosystem II. J Am Chem Soc. 2017; 139:1718–1721. [PubMed: 28102667]

Author Manuscript Author Manuscript Author Manuscript Author Manuscript

26. Debus RJ. Protein ligation of the photosynthetic oxygen-evolving center. Coord Chem Rev. 2008; 252:244–258. [PubMed: 18496594]
27. Noguchi T. FTIR detection of water reactions in the oxygen-evolving centre of photosystem II. Philos Trans R Soc, B. 2008; 363:1189–1195.
28. Noguchi T. Fourier transform infrared analysis of the photosynthetic oxygen-evolving center. Coord Chem Rev. 2008; 252:336–346.
29. Noguchi T. Fourier transform infrared difference and time-resolved infrared detection of the electron and proton transfer dynamics in photosynthetic water oxidation. Biochim Biophys Acta, Bioenerg. 2015; 1847:35–45.
30. Haumann M, Müller C, Liebisch P, Iuzzolino L, Dittmer J, Grabolle M, Neisius T, Meyer-Klaucke W, Dau H. Structural and oxidation state changes of the photosystem II manganese complex in four transitions of the water oxidation cycle (S0→ S1, S1→ S2, S2→ S3, and S3, 4→ S0) characterized by X-ray absorption spectroscopy at 20 K and room temperature. Biochemistry. 2005; 44:1894–1908. [PubMed: 15697215]
31. Yano J, Kern J, Sauer K, Latimer MJ, Pushkar Y, Biesiadka J, Loll B, Saenger W, Messinger J, Zouni A, Yachandra VK. Where water is oxidized to dioxygen: structure of the photosynthetic Mn4Ca cluster. Science. 2006; 314:821–825. [PubMed: 17082458]
32. Dau H, Grundmeier A, Loja P, Haumann M. On the structure of the manganese complex of photosystem II: extended-range EXAFS data and specific atomic-resolution models for four S-states. Philos Trans R Soc, B. 2008; 363:1237–1244.
33. Pushkar Y, Yano J, Sauer K, Boussac A, Yachandra VK. Structural changes in the Mn4Ca cluster and the mechanism of photosynthetic water splitting. Proc Natl Acad Sci U S A. 2008; 105:1879–1884. [PubMed: 18250316]
34. Sauer K, Yano J, Yachandra VK. X-ray spectroscopy of the photosynthetic oxygen-evolving complex. Coord Chem Rev. 2008; 252:318–335. [PubMed: 19190720]
35. Yano J, Yachandra VK. Where water is oxidized to dioxygen: structure of the photosynthetic Mn4Ca cluster from X-ray spectroscopy. Inorg Chem. 2008; 47:1711. [PubMed: 18330965]
36. Grundmeier A, Dau H. Structural models of the manganese complex of photosystem II and mechanistic implications. Biochim Biophys Acta, Bioenerg. 2012; 1817:88–105.
37. Glöckner C, Kern J, Broser M, Zouni A, Yachandra V, Yano J. Structural changes of the oxygen-evolving complex in photosystem II during the catalytic cycle. J Biol Chem. 2013; 288:22607–22620. [PubMed: 23766513]
38. Åhrling KA, Peterson S, Styring S. An oscillating manganese electron paramagnetic resonance signal from the S0 state of the oxygen evolving complex in photosystem II. Biochemistry. 1997; 36:13148–13152. [PubMed: 9376375]
39. Messinger J, Nugent JH, Evans MC. Detection of an EPR multiline signal for the S0* state in photosystem II. Biochemistry. 1997; 36:11055–11060. [PubMed: 9333322]
40. Messinger J, Robblee JH, Yu WO, Sauer K, Yachandra VK, Klein MP. The S0 state of the oxygen-evolving complex in photosystem II is paramagnetic: detection of an EPR multiline signal. J Am Chem Soc. 1997; 119:11349–11350. [PubMed: 25221336]
41. Peloquin JM, Campbell KA, Randall DW, Evanchik MA, Pecoraro VL, Armstrong WH, Britt RD. 55Mn ENDOR of the S2-state multiline EPR signal of photosystem II: implications on the structure of the tetranuclear Mn cluster. J Am Chem Soc. 2000; 122:10926–10942.
42. Britt RD, Campbell KA, Peloquin JM, Gilchrist ML, Aznar CP, Dicus MM, Robblee J, Messinger J. Recent pulsed EPR studies of the photosystem II oxygen-evolving complex: implications as to water oxidation mechanisms. Biochim Biophys Acta, Bioenerg. 2004; 1655:158–171.
43. Haddy A. EPR spectroscopy of the manganese cluster of photosystem II. Photosynth Res. 2007; 92:357–368. [PubMed: 17551843]
44. Kulik LV, Epel B, Lubitz W, Messinger J. Electronic structure of the Mn4OxCa cluster in the S0 and S2 States of the oxygen-evolving complex of photosystem II based on pulse 55Mn-ENDOR and EPR spectroscopy. J Am Chem Soc. 2007; 129:13421–13435. [PubMed: 17927172]
45. Navarro MP, Ames WM, Nilsson H, Lohmiller T, Pantazis DA, Rapatskiy L, Nowaczyk MM, Neese F, Boussac A, Messinger J, Lubitz W, Cox N. Ammonia binding to the oxygen-evolving

Author Manuscript Author Manuscript Author Manuscript Author Manuscript

complex of photosystem II identifies the solvent-exchangeable oxygen bridge (μ-oxo) of the manganese tetramer. Proc Natl Acad Sci U S A. 2013; 110:15561–15566. [PubMed: 24023065]

46. Cox N, Retegan M, Neese F, Pantazis DA, Boussac A, Lubitz W. Electronic structure of the oxygen-evolving complex in photosystem II prior to OO bond formation. Science. 2014; 345:804–808. [PubMed: 25124437]
47. Stich, TA., Britt, RD. Advanced Electron Paramagnetic Resonance Studies of the Oxygen-Evolving Complex. Taylor & Francis Group, LLC; Boca Raton, FL: 2015.
48. Pérez-Navarro M, Neese F, Lubitz W, Pantazis DA, Cox N. Recent developments in biological water oxidation. Curr Opin Chem Biol. 2016; 31:113–119. [PubMed: 26994742]
49. Ascone I, Meyer-Klaucke W, Murphy L. Experimental aspects of biological X-ray absorption spectroscopy. J Synchrotron Radiat. 2003; 10:16–22. [PubMed: 12511786]
50. Eaton, GR., Eaton, SS. Foundations of Modern EPR. World Scientific; 1998.
51. Hofbauer W, Zouni A, Bittl R, Kern J, Orth P, Lendzian F, Fromme P, Witt H, Lubitz W. Photosystem II single crystals studied by EPR spectroscopy at 94 GHz: The tyrosine radical Y. Proc Natl Acad Sci U S A. 2001; 98:6623–6628. [PubMed: 11381107]
52. Blakeley MP, Langan P, Niimura N, Podjarny A. Neutron crystallography: opportunities, challenges, and limitations. Curr Opin Struct Biol. 2008; 18:593–600. [PubMed: 18656544]
53. Teixeira S, Zaccai G, Ankner J, Bellissent-Funel M, Bewley R, Blakeley M, Callow P, Coates L, Dahint R, Dalgliesh R. New sources and instrumentation for neutrons in biology. Chem Phys. 2008; 345:133–151. [PubMed: 19132140]
54. Yano J, Kern J, Irrgang KD, Latimer MJ, Bergmann U, Glatzel P, Pushkar Y, Biesiadka J, Loll B, Sauer K, Messinger J, Zouni A, Yachandra VK. X-ray damage to the Mn4Ca complex in single crystals of photosystem II: a case study for metalloprotein crystallography. Proc Natl Acad Sci U S A. 2005; 102:12047–12052. [PubMed: 16103362]
55. Niimura N. Neutrons expand the field of structural biology. Curr Opin Struct Biol. 1999; 9:602–608. [PubMed: 10508767]
56. Myles DA. Neutron protein crystallography: current status and a brighter future. Curr Opin Struct Biol. 2006; 16:630–637. [PubMed: 16963258]
57. O'Dell WB, Bodenheimer AM, Meilleur F. Neutron protein crystallography: A complementary tool for locating hydrogens in proteins. Arch Biochem Biophys. 2016; 602:48–60. [PubMed: 26592456]
58. Vandavasi VG, Langan PS, Weiss KL, Parks JM, Cooper JB, Ginell SL, Coates L. Active-site protonation states in an acyl-enzyme intermediate of a class A β-lactamase with a monobactam substrate. Antimicrob Agents Chemother. 2017; 61:e01636–16. [PubMed: 27795378]
59. Fromme P, Witt HT. Improved isolation and crystallization of photosystem I for structural analysis. Biochim Biophys Acta, Bioenerg. 1998; 1365:175–184.
60. Jordan P, Fromme P, Witt HT, Klukas O, Saenger W, Krauß N. Three-dimensional structure of cyanobacterial photosystem I at 2. 5 Å resolution. Nature. 2001; 411:909–917. [PubMed: 11418848]
61. Bittl R, Zech SG, Fromme P, Witt HT, Lubitz W. Pulsed EPR structure analysis of photosystem I single crystals: localization of the phylloquinone acceptor. Biochemistry. 1997; 36:12001–12004. [PubMed: 9340008]
62. Glusker, JP. Protein Crystallization Techniques, Strategies, and Tips. In: Bergfors, TM., editor. International University Line, 1999. ACS Publications; 2003.
63. Bergfors T. Seeds to crystals. J Struct Biol. 2003; 142:66–76. [PubMed: 12718920]
64. Watanabe M, Iwai M, Narikawa R, Ikeuchi M. Is the photosystem II complex a monomer or a dimer? Plant Cell Physiol. 2009; 50:1674–1680. [PubMed: 19667103]
65. Ibrahim M, Chatterjee R, Hellmich J, Tran R, Bommer M, Yachandra VK, Yano J, Kern J, Zouni A. Improvements in serial femtosecond crystallography of photosystem II by optimizing crystal uniformity using microseeding procedures. Struct Dyn. 2015; 2:041705. [PubMed: 26726311]
66. Krug M, Weiss MS, Heinemann U, Mueller U. XDSAPP: a graphical user interface for the convenient processing of diffraction data using XDS. J Appl Crystallogr. 2012; 45:568–572.

Author Manuscript Author Manuscript Author Manuscript Author Manuscript

67. Kabsch W. Xds. Acta Crystallogr, Sect D: Biol Crystallogr. 2010; 66:125–132. [PubMed: 20124692]
68. Coates L, Stoica A, Hoffmann C, Richards J, Cooper R. The macromolecular neutron diffractometer (MaNDi) at the Spallation Neutron Source, Oak Ridge: enhanced optics design, high-resolution neutron detectors and simulated diffraction. J Appl Crystallogr. 2010; 43:570–577.
69. Coates L, Cuneo MJ, Frost MJ, He J, Weiss KL, Tomanicek SJ, McFeeters H, Vandavasi VG, Langan P, Iverson EB. The macromolecular neutron diffractometer MaNDi at the Spallation Neutron Source. J Appl Crystallogr. 2015; 48:1302–1306.
70. Peng J, Dong N, Dong Y, Pan Z, Li W. Solubility, Metastable Zone Width, and Nucleation Kinetics of Boric Acid in the NaCl–KCl–CaCl2–H2O System. J Chem Eng Data. 2015; 60:3341–3346.
71. Hu B, Huang K, Zhang X, Zhang P, Yu S. Solubility and Seeded Metastable Zone width of functional sugar L-arabinose. Food Sci Technol, Campinas. 2015; 35:51–57.

Author Manuscript Author Manuscript Author Manuscript Author Manuscript

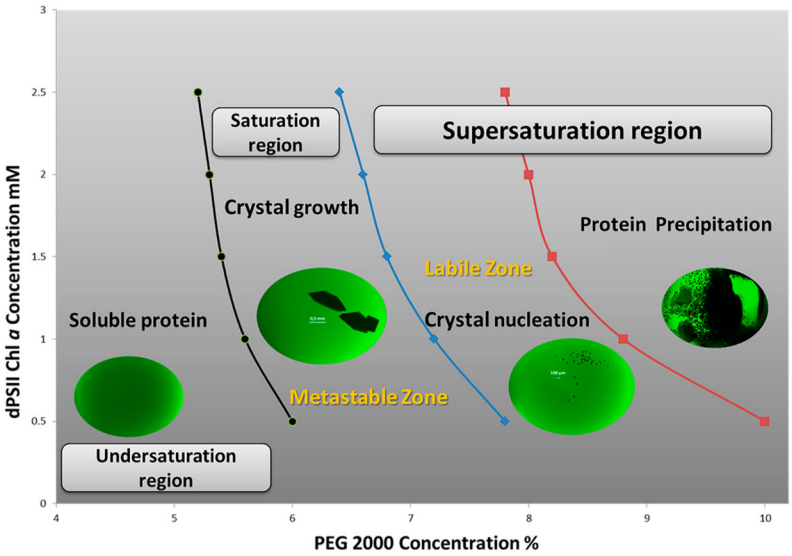

Figure 1.

Schematic phase diagram for dPSIIcc (concentration in mM Chl *a*) against PEG 2000 as a precipitant.

Author Manuscript Author Manuscript Author Manuscript Author Manuscript

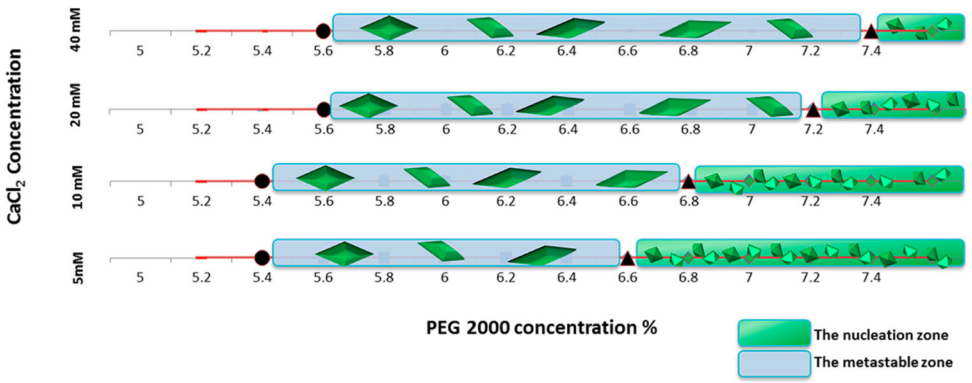

Figure 2.

Schematic diagram showing the borders between the metastable zone and either the undersaturation or the labile zone of dPSIIcc with 2 mM Chl *a* against PEG 2000 at different $CaCl_2$ concentrations. Black circles represent the PEG 2000 concentration (%) where crystals start to dissolve, whereas black triangles represent the PEG 2000 concentration at which nucleation occurs and microcrystals start growing.

Author Manuscript Author Manuscript Author Manuscript Author Manuscript

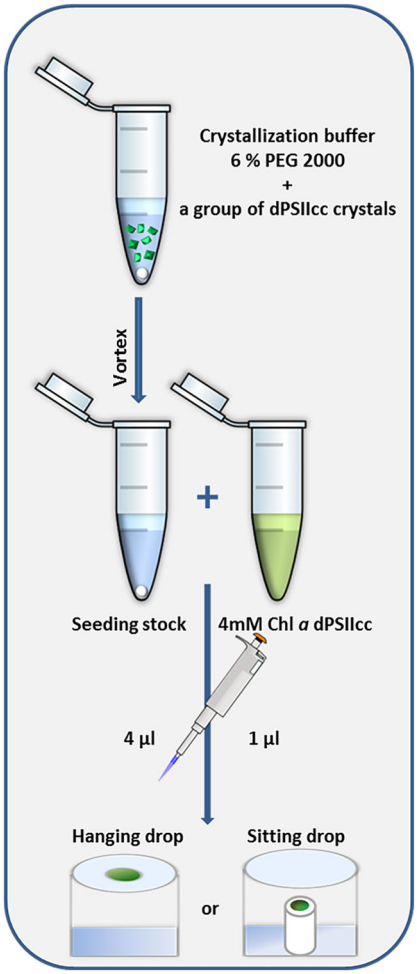

Figure 3.

Schematic illustration showing the microseeding steps. First, the seeding stock is prepared by vigorous vortexing a group of crystals in the crystallization buffer containing 6% PEG 2000 using a seeding bead. Then 4 μL of the seeding stock solution were mixed with 1 μL of the 4 mM Chl *a* dPSIIcc solution on the coverslip of the hanging drop plate or on the vessel of the sitting drop plate. The plates were left for a couple of hours to allow undisturbed crystal growth.

Author Manuscript Author Manuscript Author Manuscript Author Manuscript

Figure 4.
Medium-sized crystals of dimeric PSIIcc obtained by microseeding.

Author Manuscript Author Manuscript Author Manuscript Author Manuscript

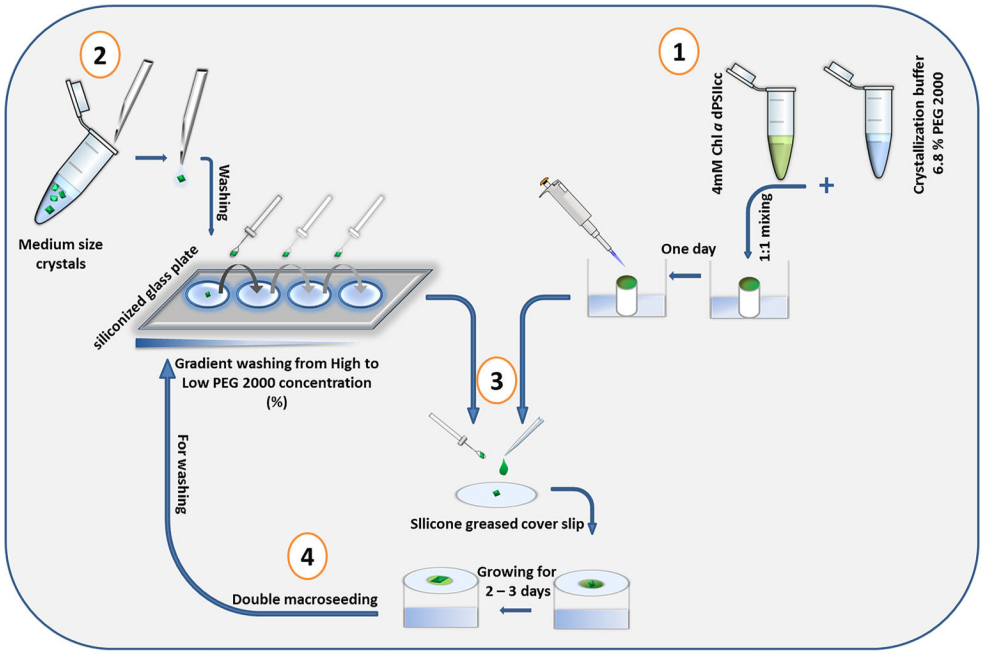

Figure 5.

Schematic representation of the macroseeding and double macroseeding method. At step one, dimeric PSIIcc was mixed 1:1 with the crystallization buffer containing 6.8% PEG 2000 in a sitting drop plate. The plate was sealed and left for 1 day to equilibrate. At the second day (step 2), each single crystal was gently transferred for washing in four steps from high to low PEG 2000. In step 3, the crystal was first washed and then transferred to a silicone-greased coverslip, where it was mixed with 4 μL of the equilibrated drop of dPSIIcc. The coverslip was quickly inverted on the hanging drop well containing 1 mL of 6.8% PEG 2000 and was left to grow for 1 week. For double macroseeding (step 4), the large crystal obtained was transferred for serial washing with repeating steps 1 and 3.

Author Manuscript Author Manuscript Author Manuscript Author Manuscript

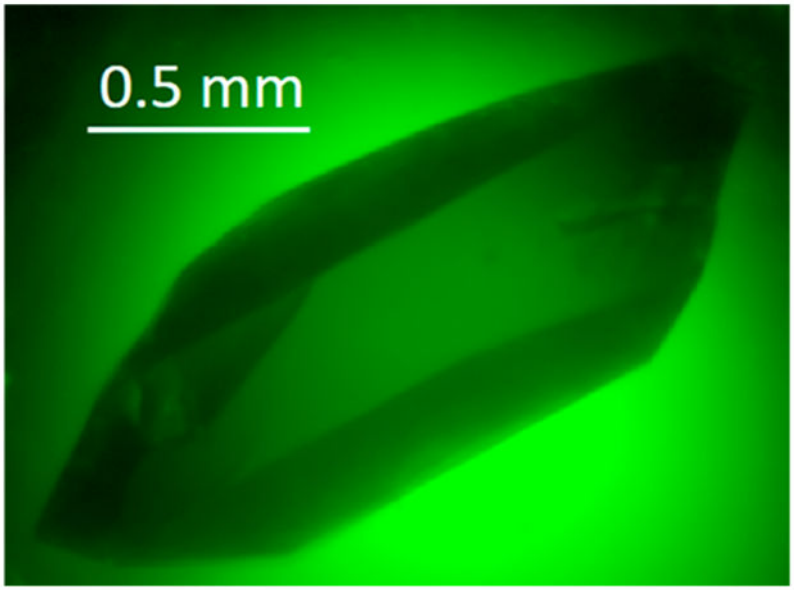

Figure 6.
Single macrocrystal of dimeric PSIIcc obtained by macroseeding.

Author Manuscript Author Manuscript Author Manuscript Author Manuscript

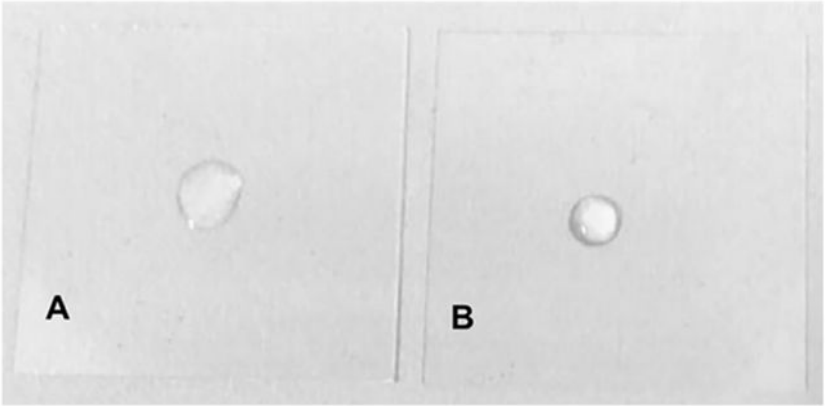

Figure 7.

Siliconized coverslip versus silicone-greased coverslip. (A) Siliconized coverslip 22 mm × 0.22 mm (Hampton, USA) with 4 μL of the crystallization buffer containing 0.015% βDM. (B) Glass coverslip 22 mm × 0.16 mm (Marienfeld, Germany) with a thin layer of silicon grease.

Author Manuscript Author Manuscript Author Manuscript Author Manuscript

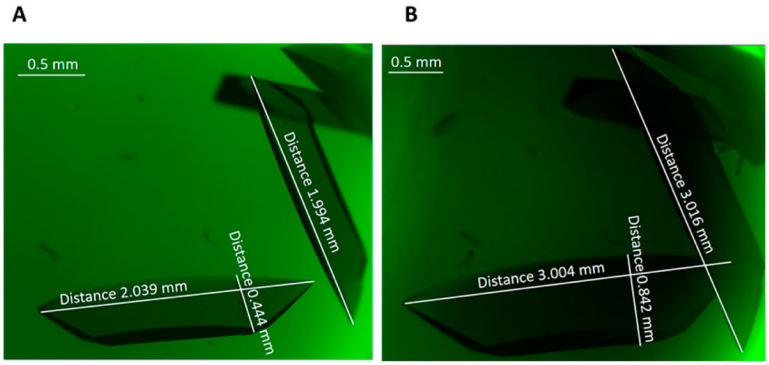

Figure 8.

Macroseeding and double macroseeding crystals of dPSIIcc. (A) Macrocrystals of dPSIIcc obtained after the first round of macroseeding and (B) the same macrocrystals after being washed and incubated with an equilibrated amount of dPSIIcc in the metastable zone.

Author Manuscript Author Manuscript Author Manuscript Author Manuscript

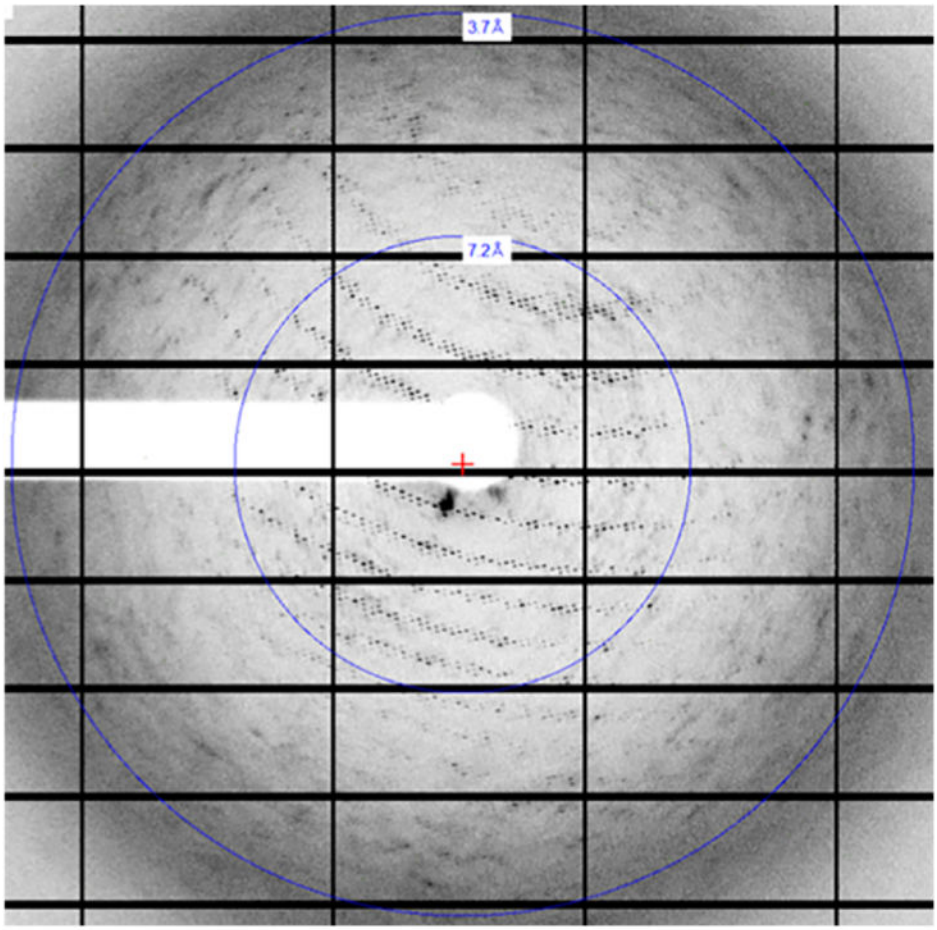

Figure 9.
XRD diffraction pattern of a dPSIIcc macrocrystal.

Author Manuscript Author Manuscript Author Manuscript Author Manuscript

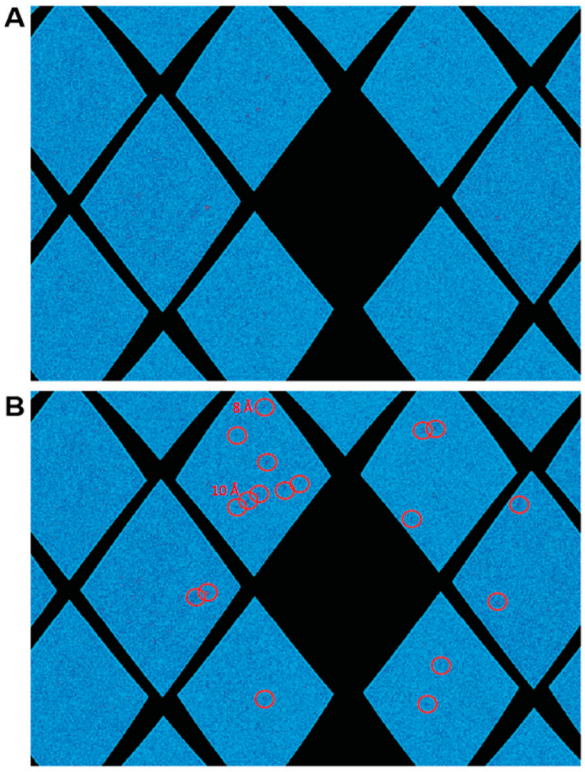

Figure 10.

Neutron diffraction pattern of a dPSIIcc macrocrystal. (A) Time-of-flight range corresponding to neutrons with wavelengths between 3.5 and 3.6 Å. For clarity, only a subset of the 40 SNS Anger cameras on MaNDi is shown. (B) Individual reffections are highlighted for better visibility, based on the wavelength and the diffraction angle of the Bragg reffections. The maximum estimated resolution of the Bragg peaks observed is 8 Å.

Author Manuscript Author Manuscript Author Manuscript Author Manuscript

Table 1

XRD Data Statistics

Data Collection	
wavelength (Å)	0.918409
space group	$P2_12_12_1$
Unit cell parameters	
a (Å)	126.59
b (Å)	223.15
c (Å)	305.46
$a = \beta = \gamma$ (deg)	90
resolution limit (Å)	49.11–4.11 (4.36–4.11)[a]
measured reffections	867591
unique reffections	66764
multiplicity	12.99
completeness (%)	97.9(88.9)
mean $I/\sigma(I)$	6.99(1.07)
R-meas (%)	34.1(237.5)
Wilson B-factor	140.12
mosaicity (deg)	0.254
$CC_{1/2}$	99.4(64.6)
ISa	11.86

[a]Data in the highest resolution shell.